Experimental decoy state BB84 quantum key distribution through a turbulent channel

Eleftherios Moschandreou, 1, * Brian J. Rollick, 1, † Bing Qi, 2, ‡ and George Siopsis 1, §

In free-space Quantum Key Distribution in turbulent conditions, scattering and beam wandering cause intensity fluctuations which increase the detected signal-to-noise ratio. This effect can be mitigated by rejecting received bits when the channel's transmittance is below a threshold. Thus, the overall error rate is reduced and the secure key rate increases despite the deletion of bits. In Decoy State BB84 QKD, several methods to find the ideal threshold have already been proposed. One promising method is the Prefixed-Threshold Real-time Selection (P-RTS) where a cutoff can be chosen prior to data collection and independently of the intensity distribution. In this work we perform finite-size Decoy State BB84 QKD in a laboratory setting where we simulate the atmospheric turbulence using an acousto-optical modulator. We show that P-RTS can yield considerably higher secure key rates, especially at higher losses. In addition, we verify that P-RTS gives a robust cutoff even when the predicted transmittance does not match the actual transmittance.

I. INTRODUCTION

As quantum communication grows from proof-ofprinciple lab demonstrations towards large-scale commercial deployment, a lot of attention is focused on the optical medium such networks can be realized on.

Today, quantum communication through fiber optical networks is possible at metropolitan scales [1, 2], but limited in distance due to transmission losses, typically ~ 0.2 dB/km at 1550 nm wavelength [3]. While classical optical signals can be enhanced by intermediate amplifiers and reach far larger distances, such techniques cannot be employed to amplify quantum signals due to the nocloning theorem [4]. Quantum repeaters [5] are a possible solution, but much progress needs to be made before they become available for practical quantum communication. Free-space channels offer an attractive alternative for intermediate distances for mobile or remote communicating parties, or as part of a ground-to-satellite network. So far, experimental demonstrations in free space include ground-to-airplane [6], hot air balloon [7], and drones [8], as well as multiple studies on the feasibility of ground-to-satellite quantum communication [7, 9–12] and the launch of a QKD dedicated satellite [13–15].

Signals traveling in free space experience losses due to turbulence, atmospheric absorption and scattering, and consequentially experience consistent degradation of the signal intensity. Caused by fluctuations in the air temperature and pressure, turbulent eddies of various sizes produce random variations in the atmospheric refractive index, which cause beam wandering and deformation of the beam front [16, 17].

The description of light propagation in a turbulent medium is a very difficult problem, but the channel can be described statistically. It is commonly accepted that the transmission coefficient can be approximated by a lognormal probability distribution at moderate turbulence [18–20], and by a gamma-gamma distribution at higher turbulence [21, 22]. However, most work to date treats the effect of turbulence on the transmittance as an average loss, without considering the details of the distribution of the transmission coefficient.

Taking the channel statistics into account, various selection methods that reject or discard recorded bits when the channel transmittance is low have been recently proposed. Evren, et al., [23] developed a signal-to-noise-ratio (SNR) filter where the detected quantum signals are grouped into bins during post-processing. Any bins with a detection rate below a certain threshold are discarded. To maximize the secure key rate, a searching algorithm was developed to find the optimal bin size and cutoff threshold.

Vallone, et al., [24] employed an auxiliary classical laser beam to probe the channel statistics, and observed good correlation between the classical and quantum transmittance data. They developed the Adaptive Real-Time Selection (ARTS) method, where the probed channel statistics are used to post-select bits recorded during high transmittance periods, above a certain transmittance threshold. Higher cutoff thresholds improve the signal-to-noise ratio at the cost of reducing the number of available signals so the optimal threshold is determined by numerically maximizing the extracted secure key in post-selection.

Wang, et al., [25] proposed the Prefixed-Real Time Selection (P-RTS) method and showed that the optimal selection threshold is insensitive to the channel statistics. Rather, it depends primarily on the receiver's detection setup characteristics (i.e., the detection efficiency and background noise) and less strongly on the intensity of the quantum signals. Thus, the threshold can be prede-

¹Department of Physics and Astronomy, University of Tennessee, Knoxville, TN 37996-1200, USA.

²Quantum Information Science Group, Computational Sciences and Engineering Division,
Oak Ridge National Laboratory, Oak Ridge, Tennessee 37831-6418, USA.

(Dated: December 9, 2020)

^{*} emoschan@vols.utk.edu

[†] brollick@vols.utk.edu

[‡] qib1@ornl.gov

[§] siopsis@tennessee.edu

termined without knowledge of the channel statistics, and the rejection of the recorded bits can be accomplished in real time without the need to store unnecessary bits or perform extra post-processing. The P-RTS method was extended to the Measurement-Device-Independent QKD (MDI QKD) [26] protocol in recent studies [27, 28]. In particular, ref. [28] highlights the importance of applying a selection method in MDI QKD as the turbulence impacts the protocol's efficiency not only through the SNR but also through the asymmetry between the channels the communicating parties (Alice and Bob) each use to access the middleman (Charles).

In this study, the P-RTS method is employed experimentally on the finite-size decoy state BB84 [29, 30] QKD protocol and compared to the optimal key rate found through ARTS. The random transmittance fluctuations caused by the atmospheric turbulence are simulated using an acousto-optical modulator (AOM). We found that the P-RTS method significantly increases the secure key rate compared to the case of not using post-selection, for a significant range of the channel's parameters.

In Section II, we review the features of the P-RTS method [25], and discuss how atmospheric effects might alter a free space communication channel. In Section III, we describe our experimental setup and procedure. We outline the key generation analysis and present our results in Section IV. Finally, in Section V we offer concluding remarks.

II. THEORY

In this Section, we review the main results of the P-RTS method [25], and discuss the atmospheric conditions which might produce our simulated effects.

A. Modeling a Turbulent Atmosphere

It is accepted that weak to moderate turbulence causes the transmittance coefficient of light propagating in air η to follow a lognormal distribution [31]. The probability density of the transmittance coefficient (PDTC) is given by:

$$p_{\eta_0,\sigma}(\eta) = \frac{1}{\sqrt{2\pi}\sigma\eta} \exp\left[-\frac{\left(\ln(\frac{\eta}{\eta_0}) + \frac{\sigma^2}{2}\right)^2}{2\sigma^2}\right]$$
(1)

where η_0 is the average loss, and σ is the log irradiance variance which characterizes the severity of the turbulence. A larger σ indicates a greater transmittance fluctuation. If the length L of the channel is known, σ for a plane wave can be calculated through the relation: $\sigma = 1.23 C_n^2 k^{7/6} L^{11/6}$, where k is the wavenumber, and C_n^2 is the refractive index structure constant, which could be measured using a scintillometer. For simplification, we assume the height of the channel is constant, so we can assume C_n^2 is constant [32]. Typical values for C_n^2

generally range from 10^{-17} to 10^{-12} (going from weak to strong turbulence), with a typical value being $\sim 10^{-15}$ [33]. According to the data provided in [34], a value of $\sigma = 0.9$ corresponds to C_n^2 on the order of 10^{-15} in a ~ 3 km channel, given our 1550 nm wavelength.

It is important to note that models often assume that turbulence only scatters the beam and a receiver is able to completely catch it [22]. The assumption is generally valid for plane waves, and holds as long as light is not scattered out of the beam, or absorbed [31]. Therefore, loss must still be built into the PDTC. Different algorithms (e.g., FASCODE [35]) have been developed to find atmospheric transmittance as a function of wavelength. FASCODE was used in [34] to determine the wavelength dependent atmospheric transmittance with high spectral resolution and in a variety of different weather and aerosol conditions. Following the tables in [34], we find that 13-17 dB of loss in the \sim 3 km channel is consistent with a 1 km meteorological visibility with 50% humidity. We achieve different losses by simulating different channel lengths 2.6 km and 3.5 km and C_n^2 , which normally varies five orders of magnitude between night and day, varies within an order of magnitude in the range under consideration, so it is a good approximation to fix $\sigma = 0.9$. Losses were chosen to highlight postselection's various impacts on the secure key rate. It only slightly improves the secure key rate in our lowest loss case, and in our highest loss channel it is necessary to generate a secure key.

B. Key Generation in a Turbulent Channel

We describe the process in which two users, Alice and Bob, are generating a shared secure key to use for their secret communication. Alice is sending phase randomized weak coherent (laser) pulses where her bits are encoded as the polarization state. Bob recieves and detects the pulses using single photon avalance detectors (SPAD).

1. Asymptotic case

Following the discussion of [25], to describe the dependence of the secure key generation rate R on the transmittance η of the atmospheric channel, we fix all Alice's decoy state parameters as well as all Bob's detection parameters (i.e., his detector's efficiencies, background noise and optical misalignment). Details about the optimization process are given in Appendix A. Then, the key rate can be written as a single function of the transmittance, $R(\eta)$. The maximum key rate $R_{\rm max}$ that can be extracted using the channel's statistics is given by the convolution of the PDTC, $p_{\eta_0,\sigma}(\eta)$ in Eq. (1) with the

rate $R(\eta)$,

$$R_{\text{max}} = \int_{0}^{1} R(\eta) p_{\eta_{0},\sigma}(\eta) d\eta$$
 (2)

While such an integration is not possible in practical applications, we can set a transmittance threshold η_T below which recorded bits are discarded and keep only a fraction $\int_{\eta_T}^1 p_{\eta_0,\sigma}(\eta) \, \mathrm{d}\eta$ of the sent signals. We treat the remaining recordings as having passed through a static channel of average transmittance $\langle \eta \rangle$, computed only from the transmittances above the threshold:

$$\langle \eta \rangle = \frac{\int_{\eta_T}^1 \eta p_{\eta_0,\sigma}(\eta) \, \mathrm{d}\eta}{\int_{\eta_T}^1 p_{\eta_0,\sigma}(\eta) \, \mathrm{d}\eta}$$
(3)

Then the postselected bits produce a key rate [25]:

$$R(\eta_T) = R(\langle \eta \rangle) \times \int_{\eta_T}^1 p_{\eta_0,\sigma}(\eta) \,d\eta$$
 (4)

Eq. (4) presents an optimization problem: higher cutoffs η_T improve the SNR for the postselected bits and, hence, the rate $R(\langle \eta \rangle)$ at the cost of reducing the available signals $\int_{\eta_T}^1 p_{\eta_0,\sigma}(\eta) \, d\eta$. The authors of [25] show that an optimal threshold η_T can be predetermined and the resulting key generation rate (4) can closely approach the ideal rate of Eq. (2) by making two key observations. Firstly, there exists a critical transmittance η_{CR} such that $R(\eta) = 0$, for $\eta < \eta_{CR}$. Thus, we have

$$R_{\text{max}} = \int_{0}^{1} R(\eta) p_{\eta_{0},\sigma}(\eta) d\eta = \int_{\eta_{CR}}^{1} R(\eta) p_{\eta_{0},\sigma}(\eta) d\eta$$
(5)

Secondly, the rate $R(\eta)$, although convex in general, approaches linearity very well. Approximating the rate $R(\eta)$ as linear, $R(\eta) \approx \alpha \cdot \eta + \beta$, we have,

$$R_{\text{max}} = \int_{\eta_{CR}}^{1} R(\eta) p_{\eta_{0},\sigma}(\eta) d\eta$$

$$\approx \int_{\eta_{CR}}^{1} \alpha \cdot \eta p_{\eta_{0},\sigma}(\eta) d\eta + \int_{\eta_{CR}}^{1} \beta \cdot p_{\eta_{0},\sigma}(\eta) d\eta$$

$$= R(\langle \eta \rangle) \times \int_{\eta_{CR}}^{1} p_{\eta_{0},\sigma}(\eta) d\eta$$
(6)

This implies that by setting our threshold to the critical value, $\eta_T = \eta_{CR}$, in Eq. (4), we achieve a very good approximation of $R_{\rm max}$. Importantly, the optimal transmittance cutoff does not depend on the channel's transmittance parameters.

2. Finite-size effects.

Taking the finite-size effects into consideration, the extracted secure key rate $R_{\text{finite-size}}$ depends also on the

number of pulses N sent by Alice. Discarding low transmittance events reduces the available postselected pulses to $N_{\rm post} = N \times \int_{\eta_T}^1 p_{\eta_0,\sigma}(\eta) \,\mathrm{d}\eta$, so the distilled secure key rate is modified to [25]:

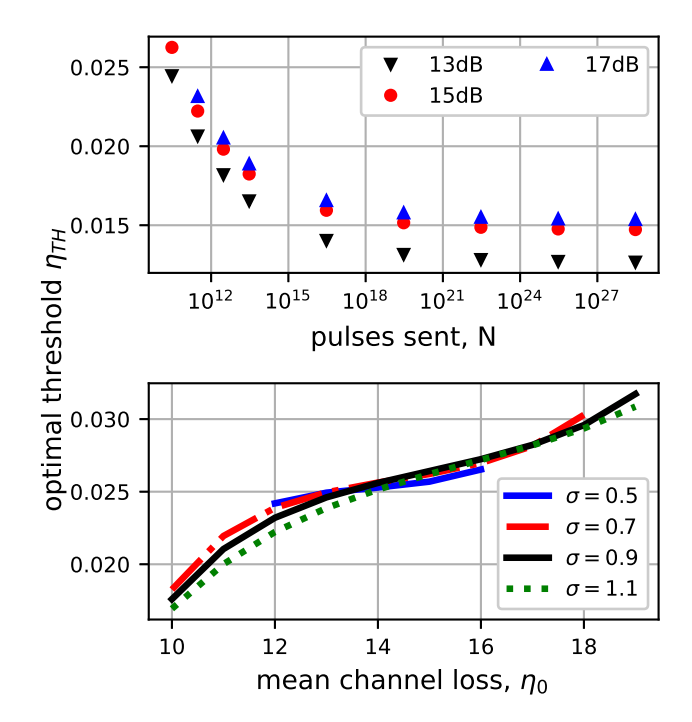


FIG. 1. Simulations. (a) The optimal transmittance threshold, for different number of sent pulses N and for different mean channel losses. $\sigma{=}0.9$. (b) The optimum threshold in terms of the mean channel loss for different σ values. $N=3\cdot10^{10}$.

$$R = R_{\text{finite-size}} (\langle \eta \rangle, N_{\text{post}}) \times \int_{\eta_{\sigma}}^{1} p_{\eta_{0}, \sigma} (\eta) \, d\eta \qquad (7)$$

The rate $R_{\text{finite-size}}$ is calculated as,

$$R_{\text{finite-size}} = \frac{\ell}{N}$$
 (8)

where ℓ the number of distilled secure bits. The latter is found from

$$\ell = s_{X,0} + s_{X,1} - s_{PA}(\phi_X) - s_{EC}(e_{obs}) , \qquad (9)$$

where $s_{X,0}$ and $s_{X,1}$ are the contributions from zero and single photon pulses, respectively, and s_{EC} and s_{PA} are the bits consumed to perform error correction and privacy amplification. The contributions $s_{X,0}$ and $s_{X,1}$, as well as the phase error ϕ_X , are estimated using the two-decoy state method [36] adapted to include finite-size effects, according to Lim, et al. [30]. The observed error e_{obs} is measured directly. Details of the secure key rate calculation are presented in Section IV.

The dependence of the rate $R_{\rm finite-size}$ given by Eq. (8) on the number of sent pulses N raises the question whether the main conclusion of the PRTS method, that the optimum transmittance threshold can be predetermined independently of the channel statistics, still holds for the case of finite number of sent pulses. Although the form of the distilled bits ℓ does not allow us to easily examine it analytically, we still can draw conclusions from numerical simulations.

The simulations results are presented in Fig. 1 for the parameters presented in tables I and II. If we consider that for a realistic application of communication time of a few minutes at frequency 1GHz we can send $\sim 10^{11}-10^{12}$ pulses, we observe that the optimum threshold at low number of sent pulses, N may differ from its asymptotic value. We also observe a rather limited variation on the optimum threshold for different values of the channel's parameters η_0 and σ . Moreover this variation does not affect the secure key generation significantly. Given these observations, we conclude that even given an imperfect knowledge of the channel statistics we can predetermine a transmittance cutoff which produces a near-optimum key generation rate. We explore this conclusion experimentally in section IV

III. EXPERIMENTAL SETUP

The experimental apparatus is shown in Fig. 2. A continuous-wave (CW) laser source (Wavelength References) at 1550.5 nm (ITU channel 33.5) is directed to a LiNbO₃ (EOSPACE) intensity modulator (IM) to carve out pulses of full width half maximum (FWHM) \sim 2 ns at a 25-MHz repetition rate. The DC bias voltage of the IM is automatically adjusted by a Null Point Controller (PlugTech) to achieve the optimal extinction ratio (typically \sim 30 dB). For each experimental session, Alice prepares and sends $N=3\times10^{10}$ pulses. To implement polarization encoding BB84, we developed a fiber based high-speed polarization modulator, following the design described in [37] and proposed in [38].

The pulses are attenuated by a combination of digital and analog variable attenuators to single-photon levels. The pulses carrying the quantum states are multiplexed on a dense wavelength division multiplexer (DWDM) (Lightel) with 1554-nm (ITU channel 29) classical laser pulses at 4-kHz repetition rate and ~ 3 ns FWHM. The classical pulses are used to probe the channel's transmittance statistics. Both sets of pulses are directed to an AOM (Brimrose) which is used to generate the random transmittance fluctuations expected from our turbulent channel. Another DWDM is employed at the receiver to separate the classical probe light and the quantum signals. The classical laser is detected by a high-gain detector (Thorlabs), and an oscilloscope (Tektronix) is used to sample and store the outputs of the detector. A 50:50 beam splitter (BS) is used to passively select Bob's detection basis, rectilinear or diagonal. Measurement in

	Y_0	b
detector H	$(7.6 \pm 0.6) \cdot 10^{-6}$	$(1.8 \pm 0.4) \cdot 10^{-4}$
${\rm detector}\ {\rm V}$	$(3.1 \pm 0.2) \cdot 10^{-5}$	$(1.8 \pm 0.4) \cdot 10^{-4}$
detector D	$(6.7 \pm 0.3) \cdot 10^{-5}$	$(2.7 \pm 0.4) \cdot 10^{-4}$
detector A	$(6.7 \pm 0.3) \cdot 10^{-5}$	$(1.8 \pm 0.4) \cdot 10^{-4}$

TABLE I. Background parameters for each detector. The input states have the same average photon number as the optimized states given in Table III. The background click probability is given by $P_{bq}(\eta) = Y_0 + b \cdot \eta$.

each basis is realized by polarizing beam splitters (PBS) and a pair of InGaAs single photon avalanche detectors (SPAD) (IDQ) gated at 25 MHz with \sim 5 ns gate width.

The detector dead-time is set to 9 μ s to reduce the afterpulse probability. Since the afterpulse probability depends on the light intensity received by the detectors, we observe a linear dependence of the background probability P_{bg} in terms of the transmittance η of the form $P_{bg}(\eta) = Y_0 + b \cdot \eta$. The parameters Y_0 and b are extracted experimentally with linear fits from test measurements and are displayed in Table I using input light with the same average photon number as that used in the experiments.

The optical misalignment is approximately 3×10^{-3} . Each SPAD is set to 10% quantum efficiency. The experimental parameters are summarized in Table II. Bob's optical efficiency refers to losses due to optical components (i.e. BS, PBS and the fiber links). The output of each SPAD is recorded by a Time Interval Analyzer (TIA) (IDQ) and a custom-made program sifts them to collect the sets nX_k, mX_k, nZ_k, mZ_k , for $k \in \{\mu_1, \mu_2, \mu_3\}$, that are needed for the secure key distillation parameters according to the model of [30]. Here, nB_k are the detections where both Alice and Bob use the same basis $B \in \{X, Z\}$ while the decoy intensity k is used, and mB_k are the detections in error for the basis B and decoy intensity k.

Bob's optical efficiency	0.42 ± 0.01
Optical misalignment	0.003 ± 0.001
Quantum efficiency (all detectors)	0.1 ± 0.05
f_{EC}	1.16
N	$3 \cdot 10^{10}$

TABLE II. Experiment parameters

Given the experimental parameters in Tables I and II, we numerically optimize the key generation to find the optimal parameters $\{q_X, P_{\mu_1}, P_{\mu_2}, \mu_1, \mu_2\}$. Here, q_X is the probability of using the rectilinear basis, P_{μ_1} and P_{μ_2} are the proportions of the signals and weak decoys, and μ_1, μ_2 are the signal and weak decoy intensities for the desired turbulence parameter set, $\{\eta_0, \sigma\}$. The vacuum decoy parameters are fixed as $P_{\mu_3} = 1 - P_{\mu_1} - P_{\mu_2}$, and $\mu_3 = 0.002$. The optimized states are presented in Table III and the details of the optimization routine are

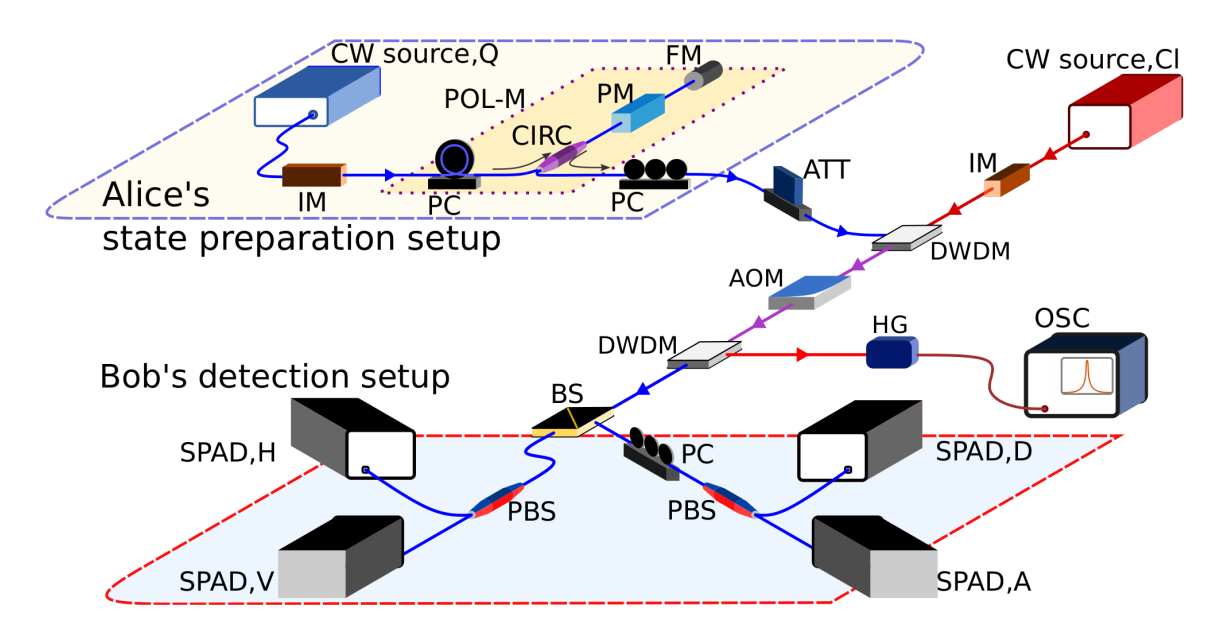


FIG. 2. A continuous wave source (CW source, Q) is used to encode the quantum states on. Pulses are carved with an intensity modulator (IM). Bits are encoded as polarization states with a polarization modulation (POL-M) setup consisting of a polarization controller (PC) a circulator (CIRC) a phase modulator (PM) and a Faraday mirror (FM). A polarization controller is used to align to the rectilinear basis. The beam is attenuated (ATT) to the desired photon number. An additional laser source (CW source,Cl) with an intensity modulator produces classical pulses that probe the channel statistics. The classical and quantum pulses are multiplexed at a dense wavelength division multiplexer (DWDM). Turbulence is simulated at an acousto-optic modulator (AOM). At Bob's side, a DWDM separates the classical and quantum signals. The high intensity classical beam is read by a high gain (HG) detector and sampled by an oscilloscope (OSC). The quantum beam is sent through a beam splitter (BS) to randomly select the measurement basis. Each polarization ,Horizontal ,Vertical ,Diagonal ,Anti-diagonal (H,V,D,A), measurement is realized by a polarization beam splitter (PBS) and a single photon avalanche detector (SPAD).

presented in Appendix A.

Turbulence	q_x	P_{μ_1}	P_{μ_2}	μ_1	μ_2
$\{\eta_0 = 10^{-1.3}, \sigma = 0.9\}$	0.879	0.610	0.215	0.56	0.23
$\{\eta_0 = 10^{-1.5}, \sigma = 0.9\}$	0.844	0.552	0.287	0.56	0.23
$\{\eta_0 = 10^{-1.7}, \sigma = 0.9\}$	0.789	0.460	0.352	0.54	0.24
$\{\eta_0 = 10^{-1.9}, \sigma = 0.9\}$	0.683	0.319	0.439	0.54	0.245

TABLE III. Alice's optimized quantum states.

IV. ANALYSIS AND RESULTS

Having collected all the sets nX_k, mX_k, nZ_k, mZ_k defined in the previous section for $k \in \{\mu_1, \mu_2, \mu_3\}$, we distill according to [30] a secure key of length ℓ ,

$$\ell = \left[s_{X,0} + s_{X,1} \left(1 - h(\phi_X) \right) - n_X \cdot f_{EC} \cdot h(e_{obs}) - 6 \log_2 \frac{21}{\varepsilon_{sec}} - \log_2 \frac{2}{\varepsilon_{cor}} \right] (10)$$

where $s_{X,0}$ and $s_{X,1}$ are the lower bounds on the number of bits generated by zero and single photon pulses

(which are immune to photon number splitting attacks) while both Alice and Bob use the rectilinear basis, ϕ_X is the upper bound on the phase error, $h(\cdot)$ is the binary entropy function,

$$h(x) = -x \log_2 x - (1-x) \log_2 (1-x) \tag{11}$$

and $e_{obs} = \frac{m_X}{n_X}$ is the quantum bit error rate, with $m_X = mX_{\mu_1} + mX_{\mu_2} + mX_{\mu_3}$, and $n_X = nX_{\mu_1} + nX_{\mu_2} + nX_{\mu_3}$. The term $-n_X \cdot f_{EC} \cdot h(e_{obs})$ describes the bits consumed by the classical error correction algorithm [39] with efficiency $f_{EC} = 1.16$, and $\varepsilon_{cor} = 10^{-15}$ is the correctness parameter. The term $-s_{X,1} \cdot h(\phi_X)$ describes the bits consumed during the privacy amplification stage to achieve secrecy according to the secrecy parameter $\varepsilon_{sec} = 10^{-10}$.

Figure 3 presents the measured secure key rates at 13, 15, and 17 dB mean turbulence loss for increasing applied transmittance cutoffs. Thus, the data points are produced using ARTS. We observe the maximum extracted rate matches the optimum cutoff given by the P-RTS method in the simulations. The error bars represent an uncertainty ± 0.005 in setting the desired signal photon number μ_1 and weak decoy photon number μ_2 given in Table III. In practical applications though, intensity uncertainties should be treated more formally with methods such as those discussed in ref. [40].

In Figure 3 the benefit of applying the Selection method is clearly demonstrated.

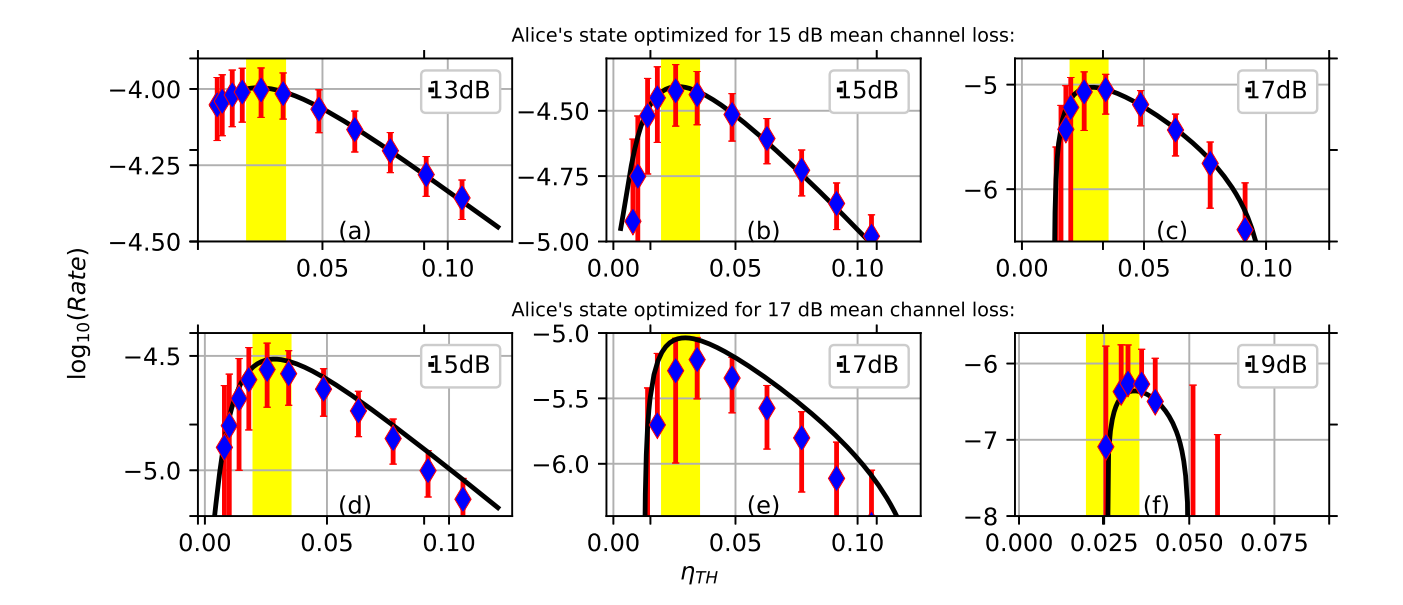


FIG. 3. First row (a)-(c): Distilled secure key rates at 13, 15 and 17dB mean channel loss for increasing applied transmittance cutoffs. The state sent by Alice is optimized for 15dB mean channel loss. Second row (d)-(f): Distilled secure key rates at 15, 17 and 19dB mean channel loss for increasing applied transmittance cutoffs. The state sent by Alice is optimized for 15dB mean channel loss. The errorbars represent a ± 0.005 uncertainty in the signal and weak decoy average photon number. The yellow shaded areas represent the range of variation on the optimal transmittance threshold, presented in Figure 1.

We observe an increase in the secure key generation and emphasize that without the selection method, the key generation for the turbulence conditions of Figure 3 beyond 15 dB average loss is zero. Thus we create "something out of nothing" as stated in [25]. At the optimal threshold at 17 dB loss, we generate 10^{-5} bits per pulse, so for this session a secure key of length $10^{-5} \times 3 \times 10^{10} = 300$ kbits can be extracted thanks to the selection method. Note, one important prediction of the P-ARTS method [25] is that the QKD parameters and optimal cutoff can be predetermined regardless of the channel statistics. This prediction is supported by our experimental results shown in Fig. 3. For example, Fig.3 (b) and Fig.3 (d) present the secure key rates over a turbulent channel with an average loss of 15dB, using QKD parameters optimized based on either a 15dB channel or 17 dB channel.

V. CONCLUDING REMARKS

In this work, we conduct an experimental demonstration of Decoy State BB84 QKD over a simulated turbulent channel taking finite-size effects into account. We show that the main conclusion of the Prefixed Real-Time Selection(P-RTS) scheme proposed in [25], that the transmittance threshold can be predetermined independently of the channel statistics, holds well in the regime of realistically finite events, further supporting the ap-

plicability of the method. The secure key rate can be significantly improved in turbulent atmospheric conditions, especially at high loss. The selection method can be easily implemented without any significant technological upgrades, and while saving computational resources. We observe that the it is especially beneficial for lower quality detection setups i.e. lower detection efficiency and/or higher detection noise as the turbulence impacts their SNR more severely.

We remark that one important assumption behind the security proof adopted in this paper is that the global phase of Alice's quantum state signal is random [41]. This could be achieved by using a PM at Alice to actively randomize the phase of each quantum signal, as demonstrated in [42]. For simplicity, we do not implement phase randomization in this work. Nevertheless, since the coherence time of Alice's laser is much smaller than the data collection time, the detection statistics observed in our experiment (thus our conclusion) would be the same as the case when phase randomization is applied.

ACKNOWLEDGMENTS

This work was supported by the U.S. Office of Naval Research under award number N00014-15-1-2646. We thank Hoi-Kwong Lo and Wenyuan Wang for useful comments, and Raphael Pooser for help with the initial setup.

- [1] M. Sasaki, M. Fujiwara, H. Ishizuka, W. Klaus, K. Wakui, M. Takeoka, S. Miki, T. Yamashita, Z. Wang, A. Tanaka, K. Yoshino, Y. Nambu, S. Takahashi, A. Tajima, A. Tomita, T. Domeki, T. Hasegawa, Y. Sakai, H. Kobayashi, T. Asai, K. Shimizu, T. Tokura, T. Tsurumaru, M. Matsui, T. Honjo, K. Tamaki, H. Takesue, Y. Tokura, J. F. Dynes, A. R. Dixon, A. W. Sharpe, Z. L. Yuan, A. J. Shields, S. Uchikoga, M. Legré, S. Robyr, P. Trinkler, L. Monat, J.-B. Page, G. Ribordy, A. Poppe, A. Allacher, O. Maurhart, T. Länger, M. Peev, and A. Zeilinger, Opt. Express 19, 10387 (2011).
- [2] Y.-L. Tang, H.-L. Yin, Q. Zhao, H. Liu, X.-X. Sun, M.-Q. Huang, W.-J. Zhang, S.-J. Chen, L. Zhang, L.-X. You, Z. Wang, Y. Liu, C.-Y. Lu, X. Jiang, X. Ma, Q. Zhang, T.-Y. Chen, and J.-W. Pan, Phys. Rev. X 6, 011024 (2016).
- [3] C. Simon, Nature Photonics 11, 678 (2017).
- [4] W. K. Wootters and W. H. Zurek, Nature 299, 802 (1982).
- [5] H.-J. Briegel, W. Dür, J. I. Cirac, and P. Zoller, Phys. Rev. Lett. 81, 5932 (1998).
- [6] S. Nauerth, F. Moll, M. Rau, C. Fuchs, J. Horwath, S. Frick, and H. Weinfurter, Nature Photonics 7, 382 EP (2013).
- [7] J.-Y. Wang, B. Yang, S.-K. Liao, L. Zhang, Q. Shen, X.-F. Hu, J.-C. Wu, S.-J. Yang, H. Jiang, Y.-L. Tang, B. Zhong, H. Liang, W.-Y. Liu, Y.-H. Hu, Y.-M. Huang, B. Qi, J.-G. Ren, G.-S. Pan, J. Yin, J.-J. Jia, Y.-A. Chen, K. Chen, C.-Z. Peng, and J.-W. Pan, Nature Photonics 7, 387 EP (2013), article.
- [8] H.-Y. Liu, X.-H. Tian, C. Gu, P. Fan, X. Ni, R. Yang, J.-N. Zhang, M. Hu, Y. Niu, X. Cao, X. Hu, G. Zhao, Y.-Q. Lu, Z. Xie, Y.-X. Gong, and S.-N. Zhu, "Dronebased all-weather entanglement distribution," (2019), arXiv:1905.09527.
- [9] J. G. Rarity, P. R. Tapster, P. M. Gorman, and P. Knight, New Journal of Physics 4, 82 (2002).
- [10] E. Meyer-Scott, Z. Yan, A. MacDonald, J.-P. Bourgoin, H. Hübel, and T. Jennewein, Phys. Rev. A 84, 062326 (2011).
- [11] G. Vallone, D. Bacco, D. Dequal, S. Gaiarin, V. Luceri, G. Bianco, and P. Villoresi, Phys. Rev. Lett. 115, 040502 (2015).
- [12] S.-K. Liao, H.-L. Yong, C. Liu, G.-L. Shentu, D.-D. Li, J. Lin, H. Dai, S.-Q. Zhao, B. Li, J.-Y. Guan, W. Chen, Y.-H. Gong, Y. Li, Z.-H. Lin, G.-S. Pan, J. S. Pelc, M. M. Fejer, W.-Z. Zhang, W.-Y. Liu, J. Yin, J.-G. Ren, X.-B. Wang, Q. Zhang, C.-Z. Peng, and J.-W. Pan, Nature Photonics 11, 509 (2017).
- [13] S.-K. Liao, W.-Q. Cai, W.-Y. Liu, L. Zhang, Y. Li, J.-G. Ren, J. Yin, Q. Shen, Y. Cao, Z.-P. Li, F.-Z. Li, X.-W. Chen, L.-H. Sun, J.-J. Jia, J.-C. Wu, X.-J. Jiang, J.-F. Wang, Y.-M. Huang, Q. Wang, Y.-L. Zhou, L. Deng, T. Xi, L. Ma, T. Hu, Q. Zhang, Y.-A. Chen, N.-L. Liu, X.-B. Wang, Z.-C. Zhu, C.-Y. Lu, R. Shu, C.-Z. Peng, J.-Y. Wang, and J.-W. Pan, Nature 549, 43 (2017).
- [14] S.-K. Liao, W.-Q. Cai, J. Handsteiner, B. Liu, J. Yin, L. Zhang, D. Rauch, M. Fink, J.-G. Ren, W.-Y. Liu, Y. Li, Q. Shen, Y. Cao, F.-Z. Li, J.-F. Wang, Y.-M. Huang, L. Deng, T. Xi, L. Ma, T. Hu, L. Li, N.-L. Liu, F. Koidl, P. Wang, Y.-A. Chen, X.-B. Wang, M. Steindor-

- fer, G. Kirchner, C.-Y. Lu, R. Shu, R. Ursin, T. Scheidl, C.-Z. Peng, J.-Y. Wang, A. Zeilinger, and J.-W. Pan, Phys. Rev. Lett. **120**, 030501 (2018).
- [15] J. Yin, Y.-H. Li, S.-K. Liao, M. Yang, Y. Cao, L. Zhang, J.-G. Ren, W.-Q. Cai, W.-Y. Liu, S.-L. Li, R. Shu, Y.-M. Huang, L. Deng, L. Li, Q. Zhang, N.-L. Liu, Y.-A. Chen, C.-Y. Lu, X.-B. Wang, F. Xu, J.-Y. Wang, C.-Z. Peng, A. K. Ekert, and J.-W. Pan, Nature 582, 501 (2020).
- [16] D. Vasylyev, A. A. Semenov, and W. Vogel, Phys. Rev. Lett. 117, 090501 (2016).
- [17] D. Vasylyev, W. Vogel, and A. A. Semenov, Phys. Rev. A 97, 063852 (2018).
- [18] P. Diament and M. C. Teich, J. Opt. Soc. Am. 60, 1489 (1970).
- [19] P. W. Milonni, J. H. Carter, C. G. Peterson, and R. J. Hughes, Journal of Optics B: Quantum and Semiclassical Optics 6, S742 (200
- [20] I. Capraro, A. Tomaello, A. Dall'Arche, F. Gerlin, R. Ursin, G. Vallone, and P. Villoresi, Phys. Rev. Lett. 109, 200502 (2012).
- [21] A. Al-Habash, L. C. Andrews, and R. L. Phillips, Optical Engineering 40, 1554 (2001).
- [22] Z. Ghassemlooy, W. Popoola, and S. Rajbhandari, Optical wireless communications: system and channel modelling with Matlab® (CRC press, 2012).
- [23] C. Erven, B. Heim, E. Meyer-Scott, J. P. Bourgoin, R. Laflamme, G. Weihs, and T. Jennewein, New Journal of Physics 14, 123018 (2012).
- [24] G. Vallone, D. G. Marangon, M. Canale, I. Savorgnan, D. Bacco, M. Barbieri, S. Calimani, C. Barbieri, N. Laurenti, and P. Villoresi, Phys. Rev. A 91, 042320 (2015).
- [25] W. Wang, F. Xu, and H.-K. Lo, Phys. Rev. A 97, 032337 (2018).
- [26] H.-K. Lo, M. Curty, and B. Qi, Phys. Rev. Lett. 108, 130503 (2012).
- [27] Z.-D. Zhu, D. Chen, S.-H. Zhao, Q.-H. Zhang, and J.-H. Xi, Quantum Information Processing 18, 33 (2018).
- [28] W. Wang, F. Xu, and H.-K. Lo, "Prefixed-threshold real-time selection for free-space measurement-deviceindependent quantum key distribution," (2019), arXiv:1910.10137 [quant-ph].
- [29] C. H. Bennett and G. Brassard, Theoretical Computer Science 560, 7 (2014).
- [30] C. C. W. Lim, M. Curty, N. Walenta, F. Xu, and H. Zbinden, Phys. Rev. A 89, 022307 (2014).
- [31] G. R. Osche, Optical detection theory for laser applications (John Wiley and Sons Inc., 2002).
- [32] S. Karp, R. M. Gagliardi, S. E. Moran, and L. B. Stotts, Optical channels: fibers, clouds, water, and the atmosphere (Springer Science & Business Media, 2013).
- [33] J. W. Goodman, Statistical optics (John Wiley & Sons, 2015).
- [34] J. Wojtanowski, M. Zygmunt, M. Kaszczuk, Z. Mierczyk, and M. Muzal, Opto-Electronics Review 22, 183 (2014).
- [35] H. Smith, D. Dube, M. Gardner, S. Clough, and F. Kneizys, FASCODE-fast atmospheric signature code (spectral transmittance and radiance), Tech. Rep. (VISI-DYNE INC BURLINGTON MA, 1978).
- [36] X. Ma, B. Qi, Y. Zhao, and H.-K. Lo, Phys. Rev. A 72, 012326 (2005).

- [37] Z. Tang, Z. Liao, F. Xu, B. Qi, L. Qian, and H.-K. Lo, Phys. Rev. Lett. 112, 190503 (2014).
- [38] I. Lucio-Martinez, P. Chan, X. Mo, S. Hosier, and W. Tittel, New Journal of Physics 11, 95001 (2009).
- [39] G. Brassard and L. Salvail, in Advances in Cryptology — EUROCRYPT '93, edited by T. Helleseth (Springer Berlin Heidelberg, Berlin, Heidelberg, 1994) pp. 410–423.
- [40] A. Mizutani, M. Curty, C. C. W. Lim, N. Imoto, and K. Tamaki, New Journal of Physics 17, 093011 (2015).
- [41] H.-K. Lo and J. Preskill, arXiv preprint quantph/0610203 (2006).
- [42] Y. Zhao, B. Qi, and H.-K. Lo, Applied physics letters 90, 044106 (2007).

Appendix A: Optimizing Secure Key Rate

Decoy state QKD introduces additional degrees of freedom for the pulses sent. Optimization of these parameters can have a profound effect on the secure key rate. In this appendix, we explain how the secure key rate is calculated and describe the optimization process. We assume that Alice has full knowledge of Bob's detection setup parameters, as summarized in Tables II. She knows that Bob will apply a selection threshold and she also knows the channel's statistics $\{\eta_0, \sigma\}$. For the rest of the section, we follow the notation of Lim, et al. [30], where X denotes the rectilinear (computational) basis and Zthe diagonal (Hadamard) basis. Alice performs a numerical optimization over the free parameters of her state, $\{q_X, P_{\mu_1}, P_{\mu_2}, \mu_1, \mu_2\}$, where q_X is the fraction of bits encoded in the X-basis, P_{μ_1} and P_{μ_2} are the fractions of signal state and weak decoy state bits, respectively, μ_1 and μ_2 are the photon numbers per pulse for the signal and weak decoy states, respectively. For the vacuum decoy

state we have fixed $\mu_3 = 0.002$, and $P_{\mu_3} = 1 - P_{\mu_1} - P_{\mu_2}$. The detection probability for $k \in \{\text{signal,weak,vacuum}\}$ at the ith detector, where $i \in \{H, V, D, A\}$:

$$P_{\text{click}}^{i}\left(\mu_{k}\right) = 1 - \left(1 - p_{bg}^{i}\right) \cdot e^{-\eta_{SYS}^{i} \cdot \mu_{k}} \tag{A1}$$

The error probability is

$$E^{i}\left(\mu_{k}\right) = 1 - \left(1 - p_{bg}^{\perp i}\right) \cdot e^{-e_{mis}\eta_{SYS}^{\perp i} \cdot \mu_{k}} \tag{A2}$$

where η_{SYS}^i is the total transmission leading to detector i (i.e. channel transmittance, Bob's optical instruments and the detector's quantum efficiency). In Eq. (A2), $p_{bg}^{\perp i}$ is the background noise on the detector orthogonal to i. We note that the background noise is taken as a linear function of the channel's transmittance η : $p_{bg} = p_{bg} (\eta) = Y_0 + b \cdot \eta$. To run the numerical optimization that returns the optimal state, we need the number $n_{X,k}$ of detections for which both Alice and Bob choose the rectilinear basis with Alice having used the decoy intensity $k \in \{\mu_1, \mu_2, \mu_3\}$, and the number $m_{X,k}$ of the erroneous detections, where both Alice and Bob choose the rectilinear basis with Alice having used the decoy intensity k. We choose to send in a total of $N=3\times 10^{10}$ pulses.

Following Lim, $et \ al.$, in [30], we use:

$$\tau_n = \sum_k \frac{e^{-k} k^n p_k}{n!} \tag{A3}$$

and

$$n_{X,k}^{\pm} := \frac{\mathrm{e}^k}{p_{\mu_k}} \left[n_{X,k} \pm \sqrt{\frac{n_X}{2} \ln \frac{21}{\epsilon_{sec}}} \right] \tag{A4}$$

 n_Z can be calculated similarly. Using these, we calculate:

$$s_{X,0} \ge \tau_0 \frac{\mu_2 n_{X,\mu_3}^- - \mu_3 n_{X,\mu_2}^+}{\mu_2 - \mu_3} \tag{A5}$$

and

$$s_{X,1} \ge \frac{\tau_1 \mu_1 [n_{X,\mu_2}^- - n_{X,\mu_3}^+ - \frac{\mu_2^2 - \mu_3^2}{\mu_3^2} (n_{X,\mu_1}^+ - \frac{s_{X,0}}{\tau_0})]}{\mu_1 (\mu_2 - \mu_3) - \mu_2^2 + \mu_3^2}$$
(A6)

It is also important to obtain the upper bound of the phase error rate for each intensity. We have:

$$\phi_X \le \frac{v_{Z,1}}{s_{Z,1}} + \gamma(\epsilon_{sec}, \frac{v_{Z,1}}{s_{Z,1}}, s_{Z,1}, s_{X,1})$$
 (A7)

and the uncertainty γ is:

$$\gamma(a, b, c, d) := \sqrt{\frac{(c+d)(1-b)b}{cd\log 2} \log_2(\frac{c+d}{cd(1-b)b} \frac{21^2}{a^2}}$$
(A8)

Applying the finite-size key distillation method discussed in ref. [30], we calculate the secure key rate $R=\frac{\ell}{N}$, where ℓ is the number of distilled bits,

$$\ell = \left[s_{X,0} + s_{X,1} \left(1 - h(\phi_X) \right) - n_X \cdot f_{EC} \cdot h(e_{obs}) - 6 \log_2 \frac{21}{\varepsilon_{sec}} - \log_2 \frac{2}{\varepsilon_{cor}} \right] (A9)$$

where $s_{X,0}$ and $s_{X,1}$ are the contributions to the key rate from zero and single photon pulses, and ϕ_X is the phase error associated with the single-photon events. Their expressions stem from the three-decoy-state method [36] extended to include finite-size effects, and are taken directly from [30]. The error correction efficiency is set to $f_{EC}=1.16$, the secrecy criterion is $\varepsilon_{sec}=10^{-10}$, and the correctness criterion is $\varepsilon_{cor}=10^{-15}$. Given the detection parameters of Table II , we run a numerical optimization for various turbulence parameters (η_0,σ) that returns the optimal state $\{q_X,P_{\mu_1},P_{\mu_2},\mu_1,\mu_2\}$. Based on these parameters we construct the waveforms for Alice's decoy and polarization sequences.

Appendix B: Estimating the channel's transmittance with classical probe pulses

Proper determination of transmittance for a given milliseconds long bin requires higher intensity probe pulses

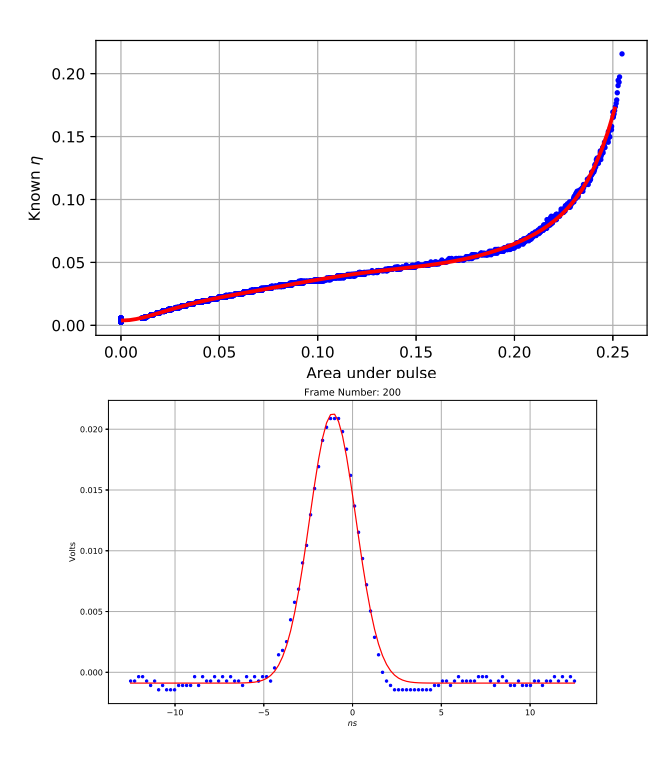


FIG. 4. (a) Polynomial Fit to determine the correlation between the measured area under the probe pulse and the programmed transmittance. (b) Example of a probed pulse captured by the oscilloscope and its Gaussian fit.

to be sent intermittently through the atmospheric channel. Beyond this, there are a number of different ways to configure the timing and measurement of the signal in the oscilloscope to the intensity of the pulse. One must choose a way which satisfies the electronic communication and memory constraints of their detection setup.

In our experiment, classical probe pulses at a 4-kHz repetition rate, and ~ 3 ns FWHM at the 29 ITU channel are sent along the quantum pulses. After passing the AOM, they are separated from the quantum pulses with a DWDM and collected by a high-gain classical photodetector. We utilize the Fast-Frame feature of a DPO 7205 Tektronix Oscilloscope, which stores samples in a short interval around the trigger (25 ns in Figure 4(b) sampled at 5 G-samples/sec). Thus, we acquire highresolution pulses (Figure 4(b)) with minimum data storage. By performing a Gaussian fit on the pulses, we acquire the area under each pulse, which is a direct measure of the transmitted intensity. For an initial calibration set, we correlate with a polynomial fit the measured pulse area with the programmed transmittance. For the actual measurements, we use this polynomial fit to deduce the transmittance given the measured pulse area.